Aluminum Incorporation into MCM-48 toward the Creation of Brønsted Acidity

Olivier Collart,[†] Pegie Cool,[†] Pascal Van Der Voort,[†] Vera Meynen,[†] Etienne F. Vansant,*[,†] Kristof Houthoofd,[‡] Piet J. Grobet,[‡] Oleg I. Lebedev,[§] and Gustaaf Van Tendeloo[§]

Laboratory of Adsorption and Catalysis, University of Antwerp, Universiteitsplein 1, B-2610 Wilrijk, Belgium, and Center for Surface Chemistry and Catalysis, Catholic University of Leuven, Kasteelpark Arenberg 23, B-3001 Leuven, Belgium, and EMAT, University of Antwerp, Groenenborgenlaan 17, B-2020 Antwerpen, Belgium

Received: January 13, 2004; In Final Form: June 30, 2004

The possibilities and limits of aluminum incorporation into the silica framework of a cubic MCM-48 have been thoroughly studied. Four different sources have been tested, namely aluminum sulfate ($Al_2(SO_4)_3$), aluminum ethoxide ($Al(Etox)_3$), aluminum isopropoxide ($Al(^iProx)_3$), and sodium aluminate ($NaAlO_2$). Only sodium aluminate has been found suitable for the incorporation, as the aluminum sulfate negatively influences the synthesis pH and both alkoxides release alcohol upon their hydrolysis, which will dissolve in the micelles, interfering in the pore arrangements inside the cubic unit cell. The sodium aluminate source permits incorporation of aluminum up to ratios of Si/Al 20 without loss of the porosity; however, a broadening of the XRD signals indicate loss of long range ordering. High-resolution electron microscopy (HRTEM) confirms this loss of long-range pore ordering but also shows the maintenance of short-range pore ordering. Correlating this with the unaltered mesoporosity indicates the preservation of a 3D pore system. An extended ^{27}Al MAS NMR study reveals that before calcination all aluminum atoms are tetrahedrally incorporated into the silicate framework. Those are situated at the surface of the framework to be compensated by surfactant cations, as no sodium was detected with ^{23}Na-MAS NMR. After calcination, about 66% of the aluminum retains its tetrahedral geometry. Those aluminum atoms are compensated by a proton provided by the decomposing surfactant during the thermal removal of the template. Brønsted groups are identified in the ^1H-MAS NMR and PAS-IR spectra at high aluminum concentration.

Introduction

For over a decade now, a large group of the material scientists have dedicated their efforts to the development of new mesoporous materials. Those materials present the particularity of combining a high specific surface area with uniformly shaped and sized pores that are ordered in a well-defined way. Those characteristics make them interesting candidates for catalysis on large molecules.

Different pore orderings have been identified from which the best known is probably the hexagonal (*p*6*m*) MCM-41 structure where the pores, all directed in one direction, form a honeycomb structure. Another known symmetry is the *Ia*3*d* designing the MCM-48 structure.[1] Such material is constructed out of cubic unit cells containing two interwoven, independent pores systems propagating in three dimensions.

Till now most of the research efforts have been focused on the hexagonal MCM-41 structure. In a first phase the attention was directed toward the rationalization of the synthesis. Later on, the silica framework was activated for eventual applications by incorporating/depositing various inorganic elements or organic molecules. Attention was also given to the characterization of every synthesized material. Multiple reviews give a good survey of the variety in the characteristics of the MCM-41 structure, all strongly depending on the synthesis method as well as the activation procedure.[2−6]

MCM-48, on the other hand, only recently received some attention from the scientific community. This is mainly due to its difficult synthesis conditions. Considerable efforts have been made till now in the optimization of the synthesis parameters with outstanding results,[7,8] but the number of publications reporting the activation of the MCM-48 by metal incorporation is rather limited. Attempts to incorporate Al[9−],[11] Mn,[11] Fe,[12] Zr,[13] Ti[14−],[16] B,[17] and V[18,19] have already been reported, but those publications represent only a few percentage of the total amount of literature concerning the activation of mesoporous structures.

Aluminum is probably one of the most studied cases in the structure activation. This is a logical continuation of the extensive studies performed since the early 1970s on the zeolitic structures, most of which are aluminosilicates.[20] Aluminum also has the advantage to be easily incorporated in the silicate framework. Despite this advantage, only few articles discuss the incorporation of aluminum into an MCM-48 structure compared to a large number of publications on MCM-41.

This article determines the limits and possibilities of aluminum incorporation into the cubic MCM-48 framework. Different aluminum sources commonly used in the literature will be tested, namely aluminum sulfate, aluminum alkoxides (aluminum ethoxide and isopropoxide), and sodium aluminate.

To favor the formation of a cubic structure, the 16-12-16 gemini surfactant is used together with the optimal synthesis parameters developed for fumed silica as the silica source.[8] The

* To whom correspondence should be adressed. E-mail: etienne.vansant@ua.ac.be. Fax: +32-3-820.23.74. Tel: +32-3-820.23.68.
[†] Laboratory of Adsorption and Catalysis, University of Antwerp.
[‡] Catholic University of Leuven.
[§] EMAT, University of Antwerp.

10.1021/jp049837x CCC: $27.50
Published on Web 08/24/2004

gemini has the intrinsic ability to favor a cubic symmetry over a wide variety of conditions.[21]

Nitrogen sorption, XR diffraction, and DRIFT are the most common characterization methods used. On a selection of samples additional characterization is performed by transmission electron microscopy (TEM),[27]Al-MAS NMR, and [1]H-MAS NMR. The latter technique is important to characterize the acid protons directly in the structure, which was not performed in former attempts.[9−11]

Experimental Section

The MCM-48 is synthesized by simultaneously dissolving the surfactant, NaOH, and the aluminum source ($Al_2(SO_4)_3$, $Al(Etox)_3$, $Al(^iProx)_3$, and $NaAlO_2$) in water under vigorous stirring.[8] After 0.5 h fumed silica (Aerosil 380) is added and the solution is stirred for another 30 min. The molar gel composition is $Si/OH^-/H_2O$/surfactant/aluminum = 1/0.26/100/0.1/*x*. Various Si/Al ratios have been used; they will be discussed below. Subsequently the gel is transferred into a Teflon-lined autoclave at 403 K for 3 days in order to synthesize the "mesogel". The gel is then recovered by filtration, washed with 15 mL of deionized water per gram of fumed silica, and resuspended in deionized water (15 g per gram of fumed silica) for 24 h at 403 K. This postsynthesis hydrothermal treatment is repeated twice. The final product is then calcined in ambient air from room temperature up to 823 K with a heating rate of 2 K/min.

The aluminum determination in the samples using a Unicam 930 AAS reveals that in all cases the aluminum dissolved in the synthesis solution is fully incorporated into the structure.

The N_2 sorption isotherms are recorded on a Quantachrome Autosorb-1-MP automated gas adsorption system. The surface area is calculated using the well-known BET method. The total pore volume is determined just after the capillary condensation step to exclude interparticle mesoporosity in the calculations. All reported pore diameters have been calculated using the NLDFT theory.[22] X-ray diffraction patterns were collected on a Philips PW1840 powder diffractometer (45 kV, 25 mA) using Ni-filtered Cu Kα radiation.

Diffuse reflectance infrared Fourier transform spectra (DRIFT spectra) were recorded on a Nicolet 20SXB FTIR spectrometer, equipped with a Spectra-Tech diffuse reflectance accessory. The resolution was 4 cm^{-1}, and 100 scans were taken of a 2 wt % diluted sample in KBr. Photoacoustic infrared spectroscopy (PAS-IR) was performed on a Nexus spectrometer bench placed in a ultradry air box and equipped with a MTEC 300 PA detection cell flushed with zeolite-dried helium. About 500 scans were taken with a resolution of 8 cm^{-1}.

TEM investigations were made on crushed samples deposited on holey carbon grids. A JEOL 4000 EX microscope operating at 400 kV and a Philips CM20 operating at 200 kV were used. The Scherzer resolution of the microscopes is 1.7 and 2.1 Å, respectively. A low intensity electron beam and medium magnifications have been used to minimize electron beam damage of the structure. The HREM images are mostly taken at large underfocus conditions where tunnels are imaged as bright dots and matter as black.[23] Fourier transformation (FT) of the HREM images is performed using the NIH Image 1.60ppc software.

The [27]Al MAS NMR spectra were recorded on a Bruker DRX400 spectrometer with a magnetic field strength of 9.4 T, and 12 000 scans were accumulated with a recycle delay time of 100 ms and a pulse length of 0.30 μs in order to fulfill the condition for the quantitative measurement of quadrupolar nuclei.[24] The sample spinning rate of the 2.5 mm rotor was 20 kHz.

The [1]H and [23]Na MAS NMR spectra were measured on a Bruker AMX300 spectrometer with a magnetic field strength of 7 T.

For the [1]H MAS NMR measurements, 32 scans were accumulated with a recycle delay time of 10 s. The [1]H MAS NMR spectra were recorded using a spin−echo sequence consisting of a $\pi/2$ pulse of 4.9 μs, an echo delay time of 100 μs, and a π pulse of 9.8 μs. For the [23]Na MAS NMR measurement, 10 000 scans were accumulated with a recycle delay time of 100 ms and a pulse length of 12 μs. The sample spinning rate of the 4 mm rotor was 10 kHz. To remove the physisorbed water during proton NMR measurements, the sample was evacuated in a vacuum of 10^{-3} Pa while raising the temperature first to 383 K. At this temperature the sample was kept for 4 h. A second level at 673 K was maintained. The rate of raising temperature in both cases was 0.5 K/min^{-1}. After the heat treatment the powder was cooled in a vacuum to room temperature and transferred into a glovebox filled with dry N_2. In the glovebox the MAS rotor was filled for the proton NMR measurement.

Results and Discussion

1. Aluminum Sulfate. Different authors have used aluminum sulfate as aluminum source with variable success.[9,10,25,26] In this study aluminum sulfate is used to synthesize an Al−MCM-48 with a Si/Al ratio of 30 and 20 ratio. The N_2-sorption isotherms are pictured in Figure 1A. Only the low aluminum concentration (Si/Al 30, Figure 1A S30) presents the well-defined capillary condensation step, indicating the presence of well-formed mesopores. This step almost disappears at higher aluminum concentration (Si/Al 20, Figure 1A S20), and, simultaneously, a hysteresis appears at high relative pressure. Such hysteresis is most comparable to one observed in the isotherms of fumed silica.[8]

Although a good mesoporosity is suggested by the isotherm of Si/Al 30, only a weak diffraction signal is measured with XRD (Figure 1B S30), pointing toward the absence of a long range ordering.

A study of the aluminosilicate framework itself with infrared spectroscopy (Figure 1C) shows that the lack of order is also present on framework scale. The Al−MCM-48 spectrum (Figure 1C S30) shows a band at 1078 cm^{-1} in the infrared absorption region of the asymmetric stretching vibration of the silicate framework.[27,28] This absorption band lies closer to the 1100 cm^{-1} of fumed silica (Figure 1C FS) than to the 1060 cm^{-1} band for the same vibration measured in the Si−MCM-48 spectrum (Figure 1C Si48). The shorter silica bonds of the Al−MCM-48 framework correspond therefore more to bonds of amorphous silica than to those of a pure silicate MCM-48. Simultaneously, the 1240 cm^{-1} band of Al−MCM-48, assigned to surface siloxane asymmetric stretching vibrations,[8] is less intense than the one of Si−MCM-48. Its sharpness is representative for the uniformity of the vibrations and expresses thus a certain degree of crystallinity in the material. A lower intensity therefore indicates a less crystalline character.

The lack of structural long rang ordering (absence of diffraction signal in the XRD), the amorphous character of the silica infrared vibration, and the hysteresis at high relative pressure in the isotherm comparable to fumed silica suggest that part of that fumed silica has not been dissolved. This considerably hinders the formation of a well-ordered structure.

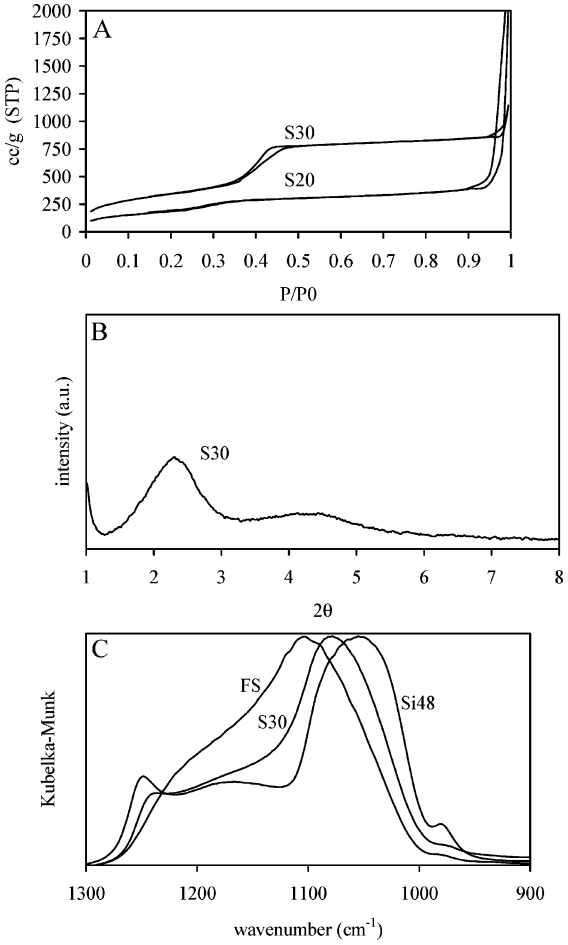

Figure 1. N_2 sorption isotherm (A), XRD (B), and DRIFT spectra (C) of an Al−MCM-48 synthesized from aluminum sulfate with a Si/Al ratio of 30 (S30) and 20 (S20). The DRIFT spectra shows also the infrared absorption region of the framework vibration of fumed silica (FS) and a pure silica MCM-48 (Si48).

TABLE 1: pH of the Gel during the Different Synthesis Steps for a Al-MCM-48 Gel Synthesized from Aluminum Sulfate with a Si/Al 30 (30) and 20 (20) Ratio and for a Pure Silica Si-MCM-48 Gel

	treatment		
	aging	1st posttreatment	2nd posttreatment
Si-MCM-48	11	10.4	9
Al-MCM-48 (30)	10.6	10	8.7
Al-MCM-48 (20)	9.6	8.7	8

The dissolving problem is a direct consequence of the use of the sulfate salt as it decomposes during its dissolution into $Al(OH)_4^-$ and HSO_4^-, as follows:

$$Al_2(SO_4)_3 + 8\,H_2O \leftrightarrow 2Al^{3+} + 8\,OH^- + 8H^+ + 3(SO_4)^{2-} \leftrightarrow 2Al(OH)_4^- + 3(HSO_4)^- + 5H^+$$

The net result is an increase of the H^+ concentration, which indisputably leads to a pH decrease. This is confirmed by pH values given in Table 1. The pH values measured after each Al−MCM-48 synthesis step are all lower compared to values noticed for the same steps in the Si−MCM-48 synthesis, and with increasing aluminum concentration a larger pH drop is noticed.

The pH values measured after the aging step as well as after the first posttreatment are close to the limits of dissolution of fumed silica.[29] A pH value of 10.6 for the Si/Al 30 is still high enough to allow silica to dissolve in order to create the mesoporous structure, but the dissolved silica particles are most probably too large to bend properly to construct curved pore walls inside the cubic unit cell (Figure 2) to create the 3D pore system. Those pores will therefore be randomly organized, resulting in an absence of any diffraction pattern in the XRD.

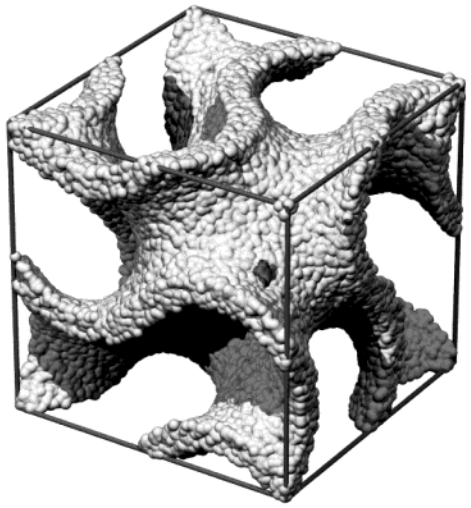

Figure 2. Representation of the pore walls within a cubic unit cell of an MCM-48.

In the case of a high aluminum concentration (Si/Al 20) the pH drop to 9.6 is much too low to induce a good dissolution of fumed silica. This completely inhibits the construction of MCM-48.

Therefore, a good structural ordering of Al−MCM-48 can only be obtained if all aluminum sources negatively influencing the pH during synthesis of the mesoporous sample are avoided. In case the aluminum source induces a pH drop, dissolution problems of silica can occur, hindering the formation of a 3D structure.

2. Alkoxides. Aluminum alkoxides have proven to be an alternative source for incorporating aluminum into the MCM-48 structure.[25,30] Those complexes easily hydrolyze, releasing only alcohol, which has no impact on the pH.

Two complexes have been tested, namely $Al(Etox)_3$ and $Al(^iProx)_3$. The first complex presents the advantage of possessing small ligands but is difficult to handle due its extremely high moisture sensitivity. The latter has the disadvantage of possessing larger ligands but can easily be handled.

In Figure 3A the N_2 sorption isotherms of the incorporated Al−MCM-48 samples with $Al(Etox)_3$ (E) and $Al(^iProx)_3$ (P) are drawn, both with a Si/Al ratio of 30 (30) and 20 (20). The comparison of the isotherms for the lowest aluminum concentration (Si/Al 30) shows that the mesoporosity of the $Al(^iProx)_3$ (P30) sample is better than the one of $Al(Etox)_3$ (E30), as it possesses a higher total pore volume and a larger pore diameter (right shift of the capillary condensation step). The difference is even more pronounced as the aluminum concentration increases. Only a small decrease in total pore volume and no change in pore diameter occurs for the isopropoxide sample (P20), where the ethoxide sample (E20) loses almost 2/3 of its mesoporosity and experiences a serious pore diameter contraction.

The same tendency in structural quality is found in the X-ray diffractograms (Figure 3B) of both the $Al(Etox)_3$ and $Al(^iProx)_3$. The diffractogram of $Al(Etox)_3$ with a Si/Al 30 ratio (E30) shows a less ordered structure, as its diffraction intensity is smaller than that of the $Al(^iProx)_3$ (P30). At higher aluminum

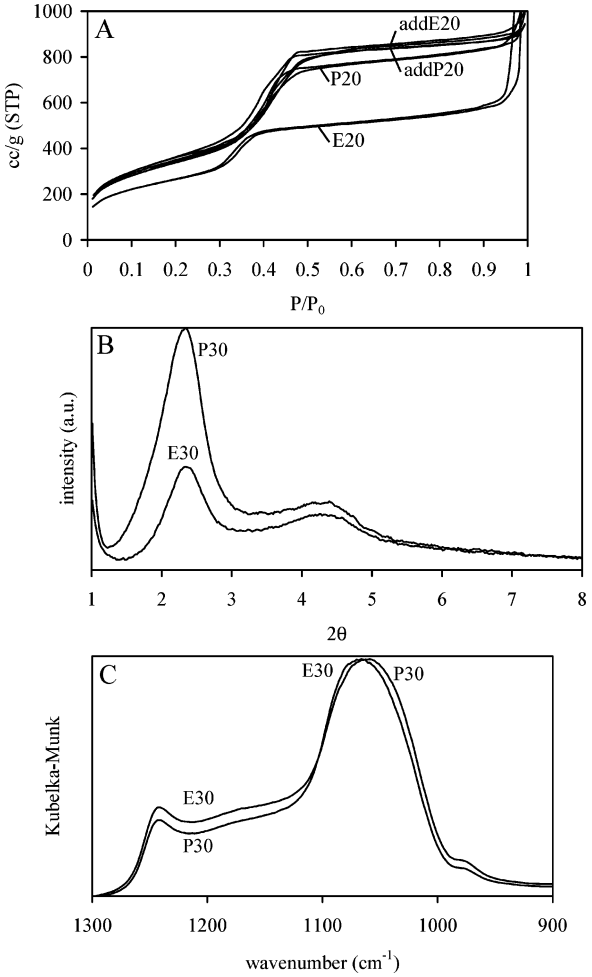

Figure 3. N_2 sorption isotherm (A), XRD (B), and DRIFT spectra (C) of an Al−MCM-48 synthesized from aluminum ethoxide with an Si/Al ratio 30 (E30) and 20 (E20) and from aluminum isopropoxide with a Si/Al ratio 30 (P30) and 20 (P20).

concentration the diffraction signals disappear completely for both samples.

The higher amorphous character of $Al(Etox)_3$ is also present on the framework level as shown by the infrared spectrum of the samples (Figure 3C). The asymmetric stretching vibration band of $Al(Etox)_3$ at 1066 cm^{-1} (E30) is closer to the amorphous structure (1100 cm^{-1}) in comparison to the $Al(^iProx)_3$ sample (1055 cm^{-1}) (P30), and the intensity of the surface siloxanes absorption band (1240 cm^{-1}) is also lower, referring to a less ordered pore surface.

Although the $Al(Etox)_3$ has the smallest ligands, it produces the least-ordered materials. This goes against the generally accepted g packing factor theory: $g = V/a^*l$. The g-factor represents the ratio of the effective volume occupied by the micelle plus any cosolvent (V) and the maximum volume that is taken by the micelle.[21] The latter is the product of the effective headgroup area (a_0) and the kinetic surfactant tail length of the micelle (l). The hydrolysis of the aluminum alkoxides releases large quantities of alcohol in the reaction medium. The partial hydrophobic character of alcohol drifts the molecules at the interface of the water−micelle medium and even further inside the micelle at higher temperatures.[31] There it will act as a cosurfactant, increasing the effective volume V and simultaneously the g-value.

To obtain the cubic MCM-48 structure the g-value should be ideally situated between 1/2 and 2/3.[21] Such a value is easily obtained using the gemini surfactant. Adding alcohol to the surfactant solution can only increase the g-value, which will disturb the formation of the cubic phase. Larger alcohol molecules will even have a greater effect on the increase of the g-value, as they are more effective in the enlargement of the V volume inside the micelle.[32] Therefore $Al(^iProx)_3$ should produce a more disordered material than $Al(Etox)_3$ due to the release of the large 2-propanol. However, the opposite result is observed.

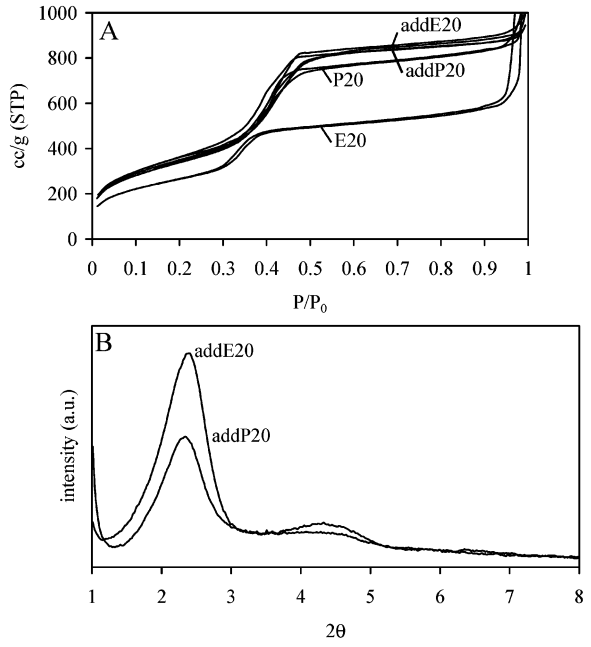

Figure 4. N_2 sorption isotherm (A) and XRD (B) of an Al−MCM-48 synthesized from sodium aluminate and added ethanol with a Si/Al 20 ratio (addE20) and from sodium aluminate and added 2-propanol with a Si/Al 20 ratio (addP20). The N_2 sorption isotherm also represents Al−MCM-48 prepared from aluminum ethoxide with an Si/Al ratio 20 (E20) and aluminum isopropoxide with a Si/Al ratio 20 (P20).

The mechanism, which causes the alkoxides to produce amorphous materials, is rather unclear. In an inverted experiment, ethanol and 2-propanol were added to the mother solution prior to an aluminosilicate gel synthesized from fumed silica and $NaAlO_2$ (vide infra). The amount of alcohol added corresponds to the same amount released by the alkoxides during the synthesis of an aluminosilicate gel with Si/Al 20 ratio. The addition of alcohol to the solution increases the pore diameter of the sample (4.7 nm against 4.4 nm without alcohol), indicating that the alcohol migrates inside the micelles causing their swelling.[33] Those pore diameters as well as the total pore volumes are larger compared to the samples synthesized without the alkoxides. This is especially the case for the sample with added ethanol which has a pore diameter of 4.7 nm and 1.22 cm^3/g total pore volume where the sample synthesized with the ethoxy source has a pore diameter of only 3.8 nm and 0.74 cm^3/g as total pore volume. This means that, although a same concentration of alcohol is present in both mother solutions, the released alcohol from the hydrolysis of alkoxides causes more problems in developing a good mesoporosity.

Although both samples with added ethanol and 2-propanol have equivalent mesoporosity, they possess different long range mesoporosity as revealed by the XRD analyses (Figure 4B). The addition of 2-propanol gives a smaller diffraction signal indicating a more disordered pore system. This is totally in line with the g packing value, as bigger alcohols playing the role of cosurfactant have a larger effect on the increase of the effective volume V.[32]

The above-mentioned results do not give a clear reason for the poorly structured meso-material. However, they give a fairly

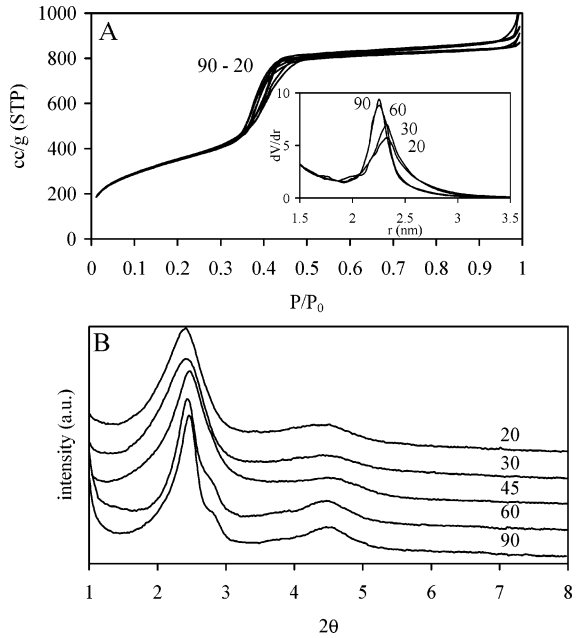

Figure 5. N_2 sorption isotherm (A) and XRD (B) of an Al−MCM-48 synthesized from sodium aluminute with Si/Al ratio from 90 to 20. The inset in part A represents the pore size distribution of the different samples with increasing aluminum ratio.

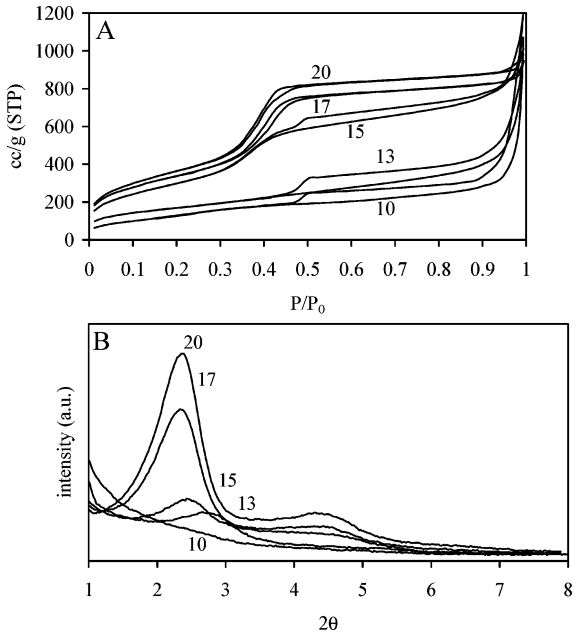

Figure 6. N_2 sorption isotherm (A) and XRD (B) of an Al−MCM-48 synthesized from sodium aluminate with Si/Al ratio from 20 to 10.

good indication that, beside the disturbing presence of alcohol,[34] other factors such as the hydrolysis behavior of the complex must interfere in the synthesis and ordering of the mesostructure. The main conclusion of these experiments is that alkoxide sources are not suitable for the synthesis of well-ordered Al−MCM-48 structures.

3. Sodium Aluminate. The above-mentioned results indicate that the ideal aluminum source should not have an influence on the pH of the mother liquid; neither should it interfere in the cubic ordering of micelles. One of the most commonly used aluminum sources in the zeolite synthesis is sodium aluminate ($NaAlO_2$).[20] Different studies have already underlined that this salt is the most suitable source for the incorporation of aluminum into the structure.[34,35] It hydrolyzes easily and forms at high pH the $Al(OH)_4^-$ anion without further influencing the pH.

The released sodium ion can even be used to compensate the negative charge of the structure caused by the replacement of the tetravalent silicon atom by a trivalent aluminum.

Figure 5A represents the different N_2 sorption isotherms of Al−MCM-48 with a decreasing Si/Al ratio from 90 to 20. Almost all isotherms are identical. Those have a pore diameter around 4.4 nm and a total pore volume of 1.22 cm^3/g. Only at low Si/Al ratio (Si/Al 30 and 20) does the slightly less steep capillary condensation step indicate a broadening of the pore size distribution (Figure 5A inset). This decline in pore uniformity is accelerated with a further increase of the aluminum concentration. The isotherms (Figure 6A) clearly show a drop of the total pore volume and an appearance of a secondary mesoporosity at Si/Al ratio 15 (interparticle mesoporosity) to even a complete vanishing of the mesoporosity at high aluminum concentration (Si/Al 10).

This loss of structural ordering is also identified in the XR diffractograms of the calcined materials (Figure 5B). Similar to the pore size distribution, an increase of the aluminum concentration induces a broadening of the XR diffraction signal. This causes a loss of resolution between the 211 and the smaller 220 diffraction signal below the Si/Al 60 ratio (Figure 5B 60). A further decrease of the Si/Al ratio below 20, enhances the broadening and decreases the intensity of the signal to its complete disappearance below Si/Al 15,[10,36] pointing out a vanishing of structural ordering (Figure 6B).

Already before calcination no clear diffraction signal is identified, indicating that the lack of cubic ordering is essentially the consequence of the inability of the gel to structure itself into a cubic system during the 3 days aging. The incorporation of aluminum into the structure can be considered as incorporating defects. All those defects have a negative influence on the formation of pore walls, as they need to be curved to form the cubic structure. This is confirmed by gradual reduction of the ordering of the cubic system with gradual increase of the aluminum content. Therefore, the aluminum content should not exceed the Si/Al 20 ratio in order to preserve mesoporosity of the Al−MCM-48 sample.

High resolution TEM images of the Si/Al 20 sample were produced (Figure 7b), to have a better understanding of the loss of structural order. The image of Figure 7b is to be compared with a HRTEM of a pure Si-MCM-48 structure (Figure 7a). The latter shows a perfectly ordered structure, and the Fourier transform (FT) can be indexed as the [33-1] zone of a cubic MCM-48 (Figure 7a inset). On the other hand, the Al−MCM-48 image shows an almost wormhole-like pore ordering. The corresponding FT pattern shows a well-defined ring pointing toward presence of some short range order (Figure 7b inset). Figure 8a shows an enlargement of the Al-MCM-48 HRTEM image. When a mask is applied in the FT pattern (Figure 8c,d) and the image is inverted, most background noise will be removed resulting in a clearer HRTEM image. Actually only the structure responsible for the ring in the FT pattern will show up (Figure 8b); other contributions, producing intensity outside the ring, are filtered out. In the present case, the resulting image will highlight the local pore ordering. In the insets 1 and 2 of Figure 8b we can find hexagonal structures as well as cubic arrangements of the pores. No dominant symmetry or long range ordering can be found. The XRD as well as the FT of the HREM however indicate a short-range pore ordering. The XRD is then to be interpreted as an indication of the distance between nearest neighbors, rather than a distance between lattice planes. The *d* value represents then the distance between the nearest pores.

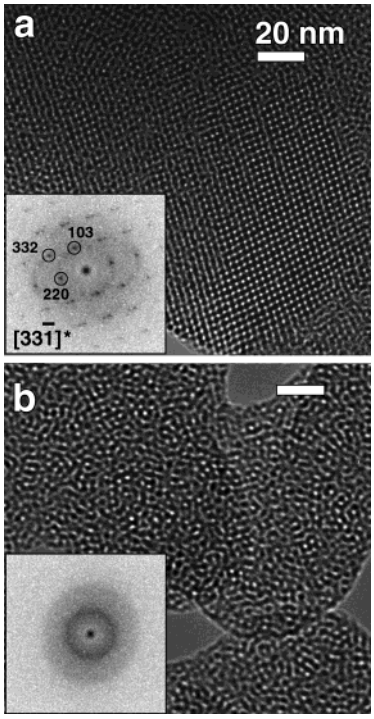

Figure 7. HRTEM of a pure silica Si−MCM-48 (a) viewed along the [33-1] axis with the FT pattern in the inset and (b) an Al−MCM-48 synthesized from sodium aluminate (Si/Al 20) with its corresponding FT pattern.

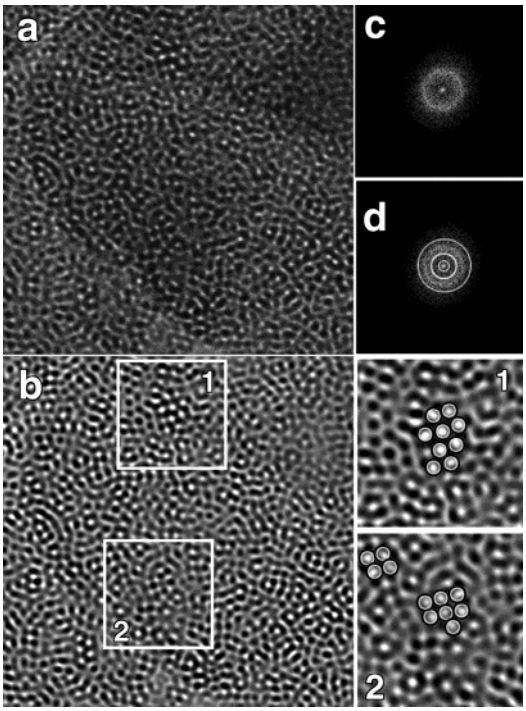

Figure 8. HRTEM magnification of Al−MCM-48 synthesized from sodium aluminate (Si/Al 20) (a) with its corresponding FT pattern (c) and the application of ring filter for a Fourier filtering (d). Filtered image of the Al−MCM-48 (b) with two enlargements (insets 1 and 2) of the zones marked with the white square frame.

The loss of the cubic ordering is a direct consequence of the aluminum incorporation into the structure. The Al−O^- bonds are longer (1.75 Å) compared to the Si−O^- bonds (1.6 Å).[37] Those longer bindings cause a distortion of the structure, preserving the short range ordering (ordering between some neighboring pores) but inducing a loss of the cubic symmetry

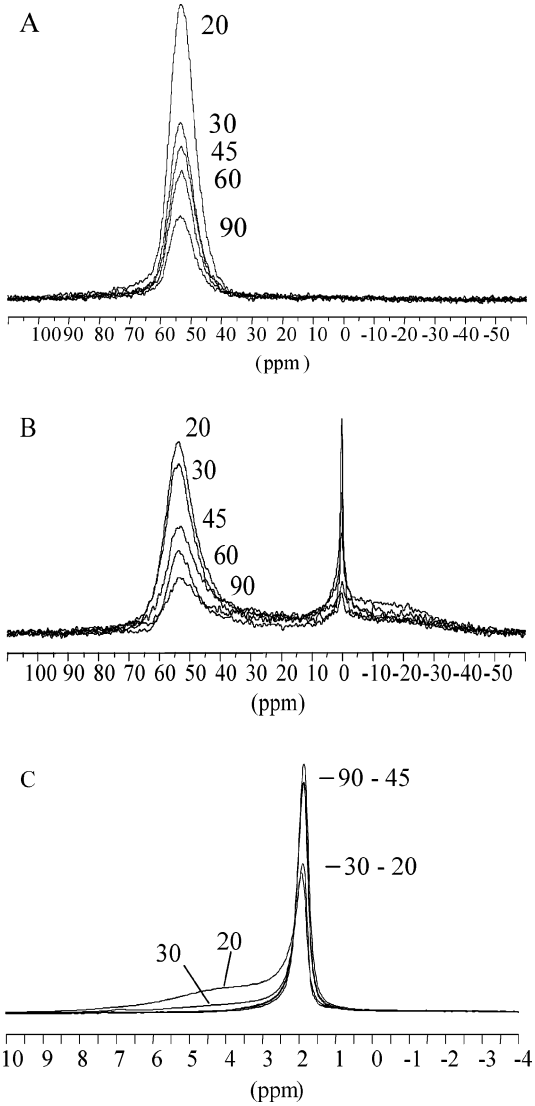

Figure 9. ^{27}Al-MAS NMR spectra of a noncalcined (A) and calcined (B) Al−MCM-48 and (c) ^{1}H spin−echo-MAS NMR of an Al−MCM-48 synthesized from sodium aluminate with a Si/Al ratio from 90 to 20.

and thus the long range ordering. Such wormhole-like pore ordering has also been found in MCM-41 with high-incorporated aluminum content.[38,39]

^{27}Al-MAS NMR analyses have been performed to analyze the effective incorporation of aluminum into the structure. Before calcination all samples present a clear and unique resonance around 53 ppm (Figure 9A). This signal is assigned to tetrahedrally coordinated aluminum, and its intensity enhances with increasing aluminum content. The absence of an octahedral coordination confirms that the framework of tetrahedral silicates has well-incorporated and dispersed the aluminum[40] as the Loewenstein rule forbids a tetrahedral configuration for two neighboring aluminum atoms.[41]

However, part of the four-coordinated aluminum is transformed to a six-coordination after calcination and appears as a signal at 0 ppm in the ^{27}Al-MAS NMR spectra of fully hydrated calcined samples (Figure 9B). An integration of the tetrahedral and octahedral signals indicates that a maximum of 45% of the aluminum is converted into the octahedral configuration and that this percentage even decreases to 33% with increasing aluminum content (Table 2). An interesting feature is that the amount of octahedral aluminum only starts to decrease at a

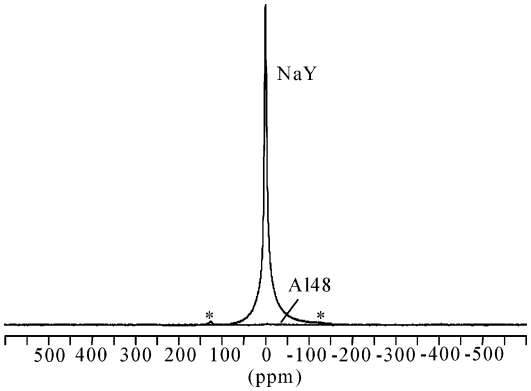

Figure 10. ^{23}Na-MAS NMR of a Al−MCM-48 synthesized from sodium aluminate with a Si/Al 30 ratio.

TABLE 2: Relative Percentage of the Aluminum Configuration for Samples Synthesized from Sodium Aluminate with Different Si/Al Ratio from 90 to 20

	% tetrahedral aluminum	% octahedral aluminum
Si/Al 90	54	46
Si/Al 60	53	47
Si/Al 45	61	40
Si/Al 30	67	33
Si/Al 20	65	36

Si/Al 60 ratio. It is also at this ratio that the 221 and the 220 XRD diffraction signals merge. This strongly suggests that the MCM-48 structure is unable to keep a well-ordered cubic symmetry with curved walls while incorporating a hetero element inside its framework. Although the MCM-48 pore walls are categorized as being amorphous, they present a more crystalline and stressed framework than common amorphous silica. This is sustained by the difference in their asymmetric infrared absorption band of the silicate framework (1100 cm^{-1} to 1050 cm^{-1}). The infrared spectrum of Si−MCM-48 has a band at lower wavenumber indicating longer and thus less stable silicate framework bonding (Figure 1C Si48) compared to the amorphous silica (Figure 1C FS), and the sharp infrared band at 1240 cm^{-1} of the Si−MCM-48 sample refers to the presence of "crystalline" surface siloxane bondings. Those are known to be more reactive,[42] which is a fairly good indication for their higher stresses. When lower aluminum concentrations are incorporated, the dominating silicate framework forces the structure to maintain its well-ordered pattern by expelling the disturbing aluminum atoms during calcination. Consequently a higher concentration of octahedral aluminum is detected. However, when the aluminum concentration increases, enough aluminum is incorporated to induce a distortion of the structure in order to decrease the structural stress caused by the longer $Al-O^-$ bonds. This distortion is reflected by a broadening of the peaks in the XRD pattern. This allows for a higher concentration of aluminum in a tetrahedral configuration.

The isomorphous substitution of silicon by aluminum inside the silica framework creates a negative overcharge, which can be compensated by sodium cations present in the synthesis solution. Figure 10 shows the ^{23}Na-MAS NMR spectra of Al−MCM-48 (Al48) after 10 000 scans and a NaY (1000 scans). The asterisks are assigned to spinning sidebands. The clear absence of any sodium signal in the spectrum of Al48 signifies that no sodium is present on the Al−MCM-48 structure and that other cations will have to compensate the overcharge. The most evident cation is the quaternary ammonium surfactant molecule with which the aluminum is able to interact strongly.[43] In this case all the aluminum must be situated at the pore wall surface to be compensated by the template molecule. This is possible, as the pore walls are no more than three atom layers thick. However, this interaction is annihilated during the calcination of the organic surfactant, but simultaneously, the thermal degradation of the template provides the necessary proton to ensure the neutrality of the structure. The particular location of this proton in the neighborhood of an aluminum atom provides the structure an acidic character.

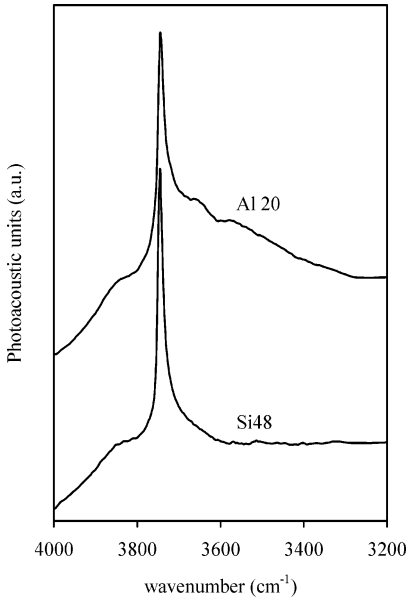

Figure 11. PA infrared spectra of a Al−MCM-48 synthesized from sodium aluminate with a Si/Al 20 ratio (Al20) and a pure silica MCM-48 (Si48).

Figure 9C shows the ^{1}H-MAS NMR spectra of the calcined samples with increasing aluminum concentration. The intense signal positioned at 2 ppm is assigned to the important presence of silanol groups on the MCM-48 structure.[44] The three lower aluminum concentrations have the same silanol signal but with the increase of the aluminum concentration below the Si/Al 30 ratio, a broad signal appears around 4 ppm at the expense of the silanol signal at 2 ppm. This signal at 4 ppm is assigned to Brønsted acid protons and has also been observed in Al−MCM-41.[44] The presence of protons of Al−OH groups cannot be excluded, but they have been detected in zeolites around 3 ppm.[45] The broadness of the line of the Brønsted acid protons at 4 ppm (Figure 9C) is caused by the rapid exchange of protons between the silanol and acid protons in the MCM-48 structure. On the other hand, the Brønsted acid protons in zeolites are isolated in the structure and give rise to a relatively sharp line. The rapid exchange with the silanols is also responsible for the difficulty of observing Brønsted signals on Al−MCM-41, contrary to the Al−MCM-48 (Figure 9C) where the silanol density is half of the MCM-41, thereby reducing the proton exchange probability and increasing by the same manner the proton signal in the ^{1}H-MAS NMR spectrum.

The presence of acid groups is also confirmed in the PAS-IR spectrum of the Si/Al 20 sample (Figure 11 Al20). The intense absorption band at 3745 cm^{-1} is assigned to free silanol groups. Those are almost exclusively present on a Si−MCM-48, showing no clear absorption band in the infrared spectrum at lower wavenumber (Figure 11 Si48). The Si/Al 20 infrared spectrum, on the other hand, shows a clear shift of those free silanol groups to the large absorption band at lower wavenumbers, meaning that some hydroxyl groups are gaining in acidic character. This confirms the presence of Brønsted acidity on the material surface. The broadness of the Brønsted hydroxyl

infrared band is also a consequence of the interactions with neighboring silanol groups as observed in the ^{1}H-MAS NMR.

The direct observation of Brønsted groups makes these materials of particular interest for acid catalysis. The presence of such groups after calcination, together with undetectable concentration of Na^+, clearly indicates that a subsequent ion-exchange procedure into the ammonium form, as performed on zeolites, is totally superfluous.

Conclusion

Not all aluminum sources are suitable for the synthesis of an Al−MCM-48, as some of them negatively influence the synthesis parameters. This is the case for the aluminum sulfate salt, which causes an important pH drop in the mother solution, seriously complicating the correct dissolution of the fumed silica. Alkoxides, on the other hand, will release alcohol upon hydrolysis of the complex. The Al ethoxide and the Al isopropoxide are only able to form a mesoporous sample at low concentration. Inverted experiments, where an amount of alcohol equivalent to the amount released by the complexes is added to the synthesis solution, give better ordered materials. This indicates that the hydrolysis of the complex has some consequence on the formation of the mesoporous structure. The most suitable aluminum source is sodium aluminate salt. Aluminum can be incorporated up to a Si/Al 20 ratio without loss of porosity. TEM and XRD suggest that the incorporation causes a disruption in the pore long range order but that the short range order is maintained. However, a Si/Al ratio below 20 induces a total collapse of the structure during the calcination procedure.

The ^{27}Al-MAS NMR spectra reveal that part of the tetrahedrally coordinated aluminum in the precursor is converted into octahedral aluminum upon calcination. At lower aluminum concentration more aluminum (45%) adopts the octahedral configuration than at higher aluminum concentration (33%). The decrease in octahedral coordination is related to the disruption of the structural order seen in the XRD. This indicates that the structure needs to adopt a more disordered character in order to stabilize the aluminum in a tetrahedral configuration. As no Na^+ ions are detected on the sample, the extra negative charge created by the incorporation of aluminum must be compensated by the cationic surfactant molecules. Those same surfactant molecules will provide the necessary charge compensating proton to the aluminum during their thermal removal. This proton possesses an acidic character which is detected in the ^{1}H-MAS NMR spectra of the highest aluminum concentration (Si/Al 30 and 20) as Brønsted groups. A broad infrared absorption band between 3700 and 3200 cm^{-1} confirms these acid sites. The broadness of the ^{1}H-MAS NMR and infrared band results from proton interactions with neighboring silanol groups. No further ion-exchange procedure is necessary to activate the structure.

Acknowledgment. The authors thank K. Schrijnemakers for providing Figure 2. P. Cool, V. Meynen, and P. J. Grobet acknowledge the FWO-Flanders Belgium for their research positions and research grants. This project has been supported by a FWO-Flanders project (no. G.0279.00) and has been performed within the IAP framework.

References and Notes

(1)) Alfredsson, V.; Anderson, M. W.; Ohsuna, T.; Terasaki, O.; Jacob, M.; Bojrup, M. *Chem. Mater.* **1997**, *9*, 2066.

(2) Corma A. *Chem. Rev.* **1997**, *97*, 2373.

(3)) Cool P.; Van Der Voort P.; Vansant E. F. Synthesis and surface modification of new inorganic porous materials. In *Encyclopedia of surface and colloid science/A*; Hubbard, Ed.; Marcel Dekker Inc.: New York, 2002; pp 5244−5256.

(4)) Trong On, D.; Desplantier-Giscard, D.; Danumah, C.; Kaliaguine, S. *Appl. Catal. A: Gen.* **2001**, *222*, 299.

(5)) Selvam, P.; Bathia, S. K.; Sonwane, C. G. *Ind. Eng. Chem. Res.* **2001**, *40*, 3237.

(6)) Linssen, T.; Cassiers, K.; Cool, P.; Van Der Voort, P.; Vansant E. F. *Adv. Colloid Interface Sci.* **2003**, *103*, 121−147.

(7)) Van Der Voort, P.; Mathieu, M.; Mees, F.; Vansant, E. F. *J. Phys. Chem. B* **1998**, *102*, 8847.

(8)) Collart O.; Van Der Voort, P.; Vansant, E. F.; Desplantier, D.; Galarneau, A.; Di Renzo, F.; Fajula, F. *J. Phys. Chem. B* **2001**, *105*, 12771.

(9)) Schumacher, K.; von Hohenesche, C. D.; Unger, K. K.; Ulrich, R.; Du-Chesne, A.; Wiesner, U.; Spiess, H. W. *Adv. Mater.* **1999**, *11*, 1194.

(10)) Romero, A. A.; Alba, M. D.; Klinowski, J. *J. Phys. Chem. B* **1998**, *102*, 123.

(11)) Xu, J.; Luan, Z. H.; Hatrmann, M.; Kevan, L. *Chem. Mater.* **1999**, *11*, 2928.

(12)) Zhao, W.; Luo, Y. F.; Deng, P.; Li Q. Z. *Catal. Lett.* **2001**, *73*, 199.

(13)) Morey, M. S.; Stucky, G. D.; Schwarz, S.; Fröba M. *J. Phys. Chem. B* **1999**, *103*, 2037.

(14)) Morey, M. S.; O'Brien, S.; Schwarz, S.; Stucky, G. D. *Chem. Mater.* **2000**, *12*, 898.

(15)) Oye, G.; Sjoblom, J.; Stöcker M. *J. Disper. Sci. Technol.* **2000**, *21*, 229.

(16)) Chang, Z.; Kevan, L. *Langmuir* **2002**, *18*, 911.

(17)) Yuan, Z. Y.; Luo, Q.; Liu, J. Q.; Chen, T. H.; Wang, J. Z.; Li, H. X. *Micrpor. Mesopor. Mater.* **2001**, *42*, 289.

(18)) Mathieu, M.; Van Der Voort, P.; Weckhuysen, B. M.; Rao, R.; Catana, G.; Schoonheydt, R. A.; Vansant, E. F. *J. Phys. Chem B* **2001**, *105*, 3393.

(19)) Chang, Z. X.; Krishna, R. M.; Xu, J.; Koodali, R.; Kevan L. *Phys. Chem. Chem. Phys.* **2001**, *3*, 1699.

(20)) van Bekkum, H.; Flanigen, E. M.; Jacobs, P. A.; Jansen, J. C. Introduction to zeolite Science and Practice. In *Studies in Surface Science and Catalysis*; Elsevier: Amsterdam, 2001; vol. 137.

(21)) Huo, Q.; Margolese, D. I.; Stucky G. D. *Chem. Mater.* **1996**, *8*, 1147.

(22)) Ravikovitch, P. I.; Neimark A. V. *Langmuir* **2000**, *16*, 2419.

(23)) Kremer, S. P. B.; Kirschhock, C. E. A.; Aerts, A.; Villani, K.; Martens, J. A.; Lebedev, O. J.; Van Tendeloo, G. *Adv. Mater.* **2003**, *15*, 1705.

(24)) Lippmaa, E.; Samoson, A.; Mägi, M. *J. Am. Chem. Soc.* **1986**, *108*, 1730.

(25)) Reddy, K. R.; Song, C. *Catal. Lett.* **1996**, *3*, 103.

(26)) Schmidt, R.; Junggreen, H.; Stöcker, M. *Chem. Commun.* **1996**, 875.

(27)) Calabro, D. C.; Valyocsik, E. W.; Ryan, F. X. *Micropor. Mater.* **1996**; *7*, 243.

(28)) Holmes, S. M.; Zholobenko, V. L.; Thursfield, A.; Plaisted, R. J.; Cundy, C. S.; Dwyer, J. *J. Chem. Soc, Faraday Trans.* **1998**, *94*, 2025.

(29)) Iler, R. K *The Chemistry of Silica: Solubility, Polymerization, Colloid and Surface Properties, and Biochemistry*; Wiley: New York, 1979.

(30)) Tuel, A.; Gontier, S. *Chem. Mater.* **1996**, *8*, 114.

(31)) Landry, C. C.; Tolbert, S. H.; Gallis, K. W.; Monnier, A.; Stucky, G. D.; Norby, P.; Hanson, J. C. *Chem. Mater* **2001**, *13*, 1600.

(32)) Ågren, P.; Linden, M.; Rosenholm, J. B.; Schwarzenbacher, R.; Kriechbaum, M.; Amenitsch, H.; Laggner, P.; Blanchard, J.; Schüth, F. *J. Phys. Chem. B* **1999**, *103*, 5943.

(33)) Mathieu, M.; Van Bavel, E.; Van Der Voort, P.; Vansant, E. F. *Stud. Surf Sci. Catal*. **2001**, *135*, 135.

(34)) Biz, S.; White, M. G. *J. Phys. Chem. B* **1999**, *103*, 8432.

(35)) Lee, Y. S.; Surjadi, D.; Rathman J. F. *Langmuir* **1996**, *12*, 6202.

(36)) Kodenev, E. G.; Shmakov, A. N.; Derevyankin A. Y.; Lapina, O. B.; Romannikov, V. N. *J. Mol. Catal. A* **2000**, *158*, 349.

(37)) Reddy, K. M.; Song, C. *Catal Lett.* **1996**, *36*, 103.

(38)) Luan, Z.; Cheng, C.-F.; Zhou, W.; Klinowski, J. *J. Phys. Chem.* **1995**, *99*, 1018.

(39)) Cabrera, S.; El Haskouri, J.; Mendioroz, S.; Guillem, C.; LaTorre, J.; Beltran-Porter, A.; Beltran-Porter, D.; Dolores Marcos, M.; Amoros, P. *Chem. Commun.* **1999**, 1679.

(40)) Klinowski, J.; Thomas, J. M.; Fyfe, C. A.; Gobbi, G. C. *Nature* **1982**, *296*, 533.

(41)) Loewenstein, M. *Am. Mineral.* **1954**, *39*, 92.

(42)) Baltes, M.; Cassiers, K.; Van Der Voort, P.; Weckhuysen, B. M.; Schoonheydt R. A.; Vansant E. F. *J. Catal.* **2001**, *197*, 160.

(43)) Janicke, M. T.; Landry, C. C.; Christiansen, S. C.; Kumar, D.; Stucky, G. D.; Chmelka, B. F. *J. Am. Chem. Soc.* **1998**, *120*, 6940.

(44)) Luo, Q.; Deng, F.; Yuan, Z.; Yang, J.; Zhang, M.; Yue, Y.; Ye, C. *J. Phys. Chem. B* **2003**, *107*, 2435.

(45)) Brunner, E.; Karge, H. G.; Pfeifer, H. Z. *Phys. Chem.* **1992**, *176*, 173.